INTERNATIONAL ATOMIC ENERGY AGENCY

FIFTEENTH INTERNATIONAL CONFERENCE ON PLASMA PHYSICS AND CONTROLLED NUCLEAR FUSION RESEARCH

Seville, Spain, 26 September – 1 October 1994

IAEA-CN-60/ A-1-II

RECENT RESULTS ON TORE SUPRA

EQUIPE TORE SUPRA

(Presented by D. Moreau)

Association EURATOM-CEA sur la fusion
Département de Recherches sur la Fusion Contrôlée
Centre d'Etudes de Cadarache
13108 Saint-Paul-Lez-Durance Cedex, France

RECENT RESULTS ON TORE SUPRA

EQUIPE TORE SUPRA[1]
(Presented by D. Moreau)

Association EURATOM-CEA sur la fusion
Département de Recherches sur la Fusion Contrôlée
Centre d'Etudes de Cadarache
13108 Saint-Paul-Lez-Durance Cedex, France

Abstract

RECENT RESULTS ON TORE SUPRA

Recent results regarding heating, confinement, current drive and profile modifications, heat and particle exhaust are reported. Improved core confinement is obtained after pellet injection (PEP) or Lower Hybrid current drive (LHEP) and may be linked with small - or reversed - central magnetic shear. Conversely, by increasing the magnetic shear in the gradient region, both LHCD and fast wave electron heating (FWEH) have produced improved global confinement with H_{RLW} up to 2 at β_p = 1.1, and 45% of the current was carried by the bootstrap current. Fast wave current drive has been observed at the level of 80 kA in a 0.4 MA discharge. In the ergodic divertor configuration, stable radiative layers were obtained with neon injection. At least 80% of a total of 7 MW injected power were radiated without confinement degradation or impurity accumulation. Finally, the heat exhaust capability of the various actively cooled plasma facing components is briefly described.

1. INTRODUCTION

TORE SUPRA is a large superconducting Tokamak (major radius : R = 2.4 m, minor radius : a < 0.8 m) routinely operated with a toroidal magnetic field intensity $B_0 \simeq 4$ Teslas on axis. High-power Ion Cyclotron Resonant Heating (ICRH) and Lower Hybrid Current Drive (LHCD) have been used throughout the 1992-1994 experimental campaigns with powers up to 8 MW and 6 MW respectively (several second pulses) and long-pulse discharges have been produced with up to a 62 s flat-top at reduced power.

Steady-state heat and particle exhaust is now becoming one of the major

---

[1] See the Appendix.

challenge in thermonuclear fusion research. The TORE SUPRA edge plasma is controlled through a 12 m^2 graphite inner wall, a set of pump limiters and an ergodic divertor, all water cooled. This provides a unique configuration for studying the energy transfer mechanisms between the plasma and the wall by radiation and convection, their compatibility with particle exhaust, and the technology of actively cooled plasma facing components.

The recent experimental physics program has thus focussed on two major items :

i) the *improvement of plasma confinement and stability* through the control of the current density profile, with the objective of obtaining *stationary* enhanced performance regimes ;

ii) the *production of stable radiative layers* in the ergodic divertor configuration in the aim of preparing steady-state operation with reduced peak heat load on the plasma facing components.

The next section of the paper will be dedicated to general transport studies, and subjects *i)* and *ii)* will be dealt with in sections 3 and 4. Finally, the heat exhaust capability of the various actively cooled plasma facing components will be briefly described in section 5.

2. TRANSPORT STUDIES AND FLUCTUATION MEASUREMENTS

To improve our understanding of anomalous transport and its relationship with plasma turbulence, both density and magnetic fluctuations have been measured in various plasma regimes [1]. The corresponding diagnostics involve reflectometry, coherent CO_2 laser scattering and microwave cross-polarization scattering.

2.1. Ohmic and auxiliary heated limiter discharges

Ohmic plasmas generally follow the neo-Alcator confinement scaling. Up to volume-averaged electron densities of 2 x 10^{19} m^{-3} the electron thermal diffusivity (χ_e) decreases with increasing density and a similar trend is observed on the edge density fluctuations. At higher densities, no further decrease of these fluctuations is observed and χ_e also remains constant (1 m^2/s). In this "saturated" ohmic regime, the ratio between the heat and particle diffusivities, χ_e/D, is of the order of 3-4. On the opposite, the level of magnetic fluctuations always *increases* linearly with density.

In auxiliary heated plasmas (ICRH and LHCD with predominant electron heating) the magnetic fluctuations in the plasma interior increase significantly while the confinement degrades (fig. 1), which proves the full electromagnetic character of the enhanced turbulence [1-2]. Discharges with ohmic-like current

density profiles are in fairly good agreement with the Rebut-Lallia-Watkins (RLW) global scaling, especially with respect to the density dependence. The RLW expression for the local heat diffusivity [3] also fits satisfactorily the experimental data at high power, when the electron temperature gradient is larger than the predicted critical gradient (∇T_c). The agreement is not so good when ∇T_e is close to ∇T_c (i.e. at low power) which suggests that the RLW expression of the critical gradient could be inaccurate. Including a simple magnetic shear dependence in it would indeed lead to a better agreement [4].

2.2. Confinement in the ergodic divertor configuration

When a resonant magnetic perturbation ($q \approx 3$) of sufficient amplitude is applied through a set of ergodic divertor (ED) coils [5], the magnetic field lines become quasi stochastic within the edge plasma layers. Due to increased electron losses in this region, the radial electric field profile is strongly modified as deduced from the analysis of the Doppler shifted density fluctuation spectra and confirmed by rotation measurements. The electric shear layer (E-field reversal) is pushed inwards at a normalized minor radius $r/a \approx 0.8$ where a thermal barrier is created. Inside this radius, the temperature profiles and the transport coefficients are basically unchanged, but the electron temperature gradient just outside $r/a \approx 0.8$ reaches values larger than 5.2 keV/m at the border of the stochastic layer in which both the temperature and its gradient are small (fig. 2a). The density gradient at the edge is weakly affected. The temperature pedestal indicates a strong reduction of the heat diffusivity near the electric shear layer. This is correlated with a significant reduction of the density fluctuation level in the region $r/a > 0.8$ as seen from both reflectometry measurements (fig. 2b) and coherent scattering (fig. 2c) [1]. As far as the global confinement is concerned, and thanks to the thermal barrier, these discharges are similar to limiter discharges in that they still follow the RLW scaling despite the magnetic field stochasticity in the outer plasma layers.

3. IMPROVED CONFINEMENT REGIMES

3.1. Pellet enhanced performance (PEP)

As in JET, pellet enhanced performance has been observed (fig. 3) during which the fusion product $n_{i0}T_{i0}\tau_E$ reaches a peak value of 1.1×10^{20} m^{-3}.keV.s [6]. This was obtained at 4 Teslas/1.3 MA with 3 MW of ICRH heating following a fast pellet injection in the plasma core (pellet velocities up to 3.3 km/s were achieved in the plasma with a two-stage pneumatic injector). The density on axis was transiently raised above 2×10^{20} m^{-3}, producing a peaked

density profile and a central magnetic shear reversal. Code simulations (LOCO, TRANSP) indicate a local reduction of the heat diffusivity [1].

3.2. Steady-state lower hybrid enhanced performance (LHEP)

A stationary improved confinement regime named "LHEP" has been observed when the current density and electron temperature profiles are strongly decoupled. This occurs when sufficient LH power drives most of the plasma current non-inductively ($P_{LH} > 2.5$ MW for $Ip \leq 0.8$ MA, $n_e(0) \approx 2.5 - 3 \times 10^{19}$ m^{-3}). The LHEP regime is characterized by an increase of the magnetic shear and a decrease of the heat diffusivity in the gradient zone, and by a flattening - and sometimes reversal - of the q-profile in the centre (fig. 4a). It leads to peaked electron pressure profiles ($T_{e0} \approx 6$-10 keV) despite a slightly off-axis power deposition from which a very low value of the core thermal diffusivity is inferred (fig. 4b) [7]. The electron thermal energy content exceeds the RLW prediction by a factor $H_{RLW} \approx 1.5$ at 4 teslas while $\beta_p \approx 0.5$. The discharges are found to be stable with respect to ballooning modes and TRANSP analysis indicates that the central core of the plasma ($r/a < 0.25$) provides access to the second stability regime.

At $I_p = 0.6$ MA, many discharges exhibited steady (m=2 dominated) MHD activity. Preliminary analysis [8] showed that ideal n = 1 infernal modes could be unstable for $\beta_p \geq 0.8$ and the stability boundary for resistive ones should be lower. Tearing or double tearing modes could also be invoked. Nevertheless, application of LHCD on high-l_i plasmas obtained with a 1.2 MA/s current ramp from 1.7 MA down to 0.6 MA led to stationary MHD-stable discharges with β_p up to 0.8 and $H_{RLW} \approx 1.6$. Those discharges which were MHD-free are found to have a smaller magnetic shear on the q=2 magnetic flux surface, similar to the 0.8 MA ones.

Another set of experiments was performed at reduced toroidal magnetic field ($B_t < 2$ Teslas) in order to produce higher normalized-β discharges ($\beta_N = \beta a B_t / I_p$). In such plasmas, LH accessibility conditions were similar to those in high-density/4-Tesla plasmas. The plasma current was varied between 0.3 MA and 0.8 MA. With LHCD alone, stable, fully non-inductive 0.4 MA discharges were obtained with β_p and β_N up to 0.8 and $H_{RLW} \approx 1.8$ (fig. 5). The bootstrap current fraction amounted roughly to 35% (fig. 6). A dependence of the MHD behaviour with respect to the phase velocity of the launched waves was observed.

3.3. Fast wave direct electron heating and current drive

Direct electron heating from the fast magnetosonic wave has been studied [4, 12] at reduced magnetic field ($B_t < 2$ Teslas) in order to maximize the single pass absorption of the wave through combined electron Landau damping and transit time magnetic pumping. The frequency was 48 MHz (dipole phasing) and the magnetic field intensity was adjusted so that the first and second harmonic cyclotron resonances of the minority hydrogen lie respectively on the inner and outer edge of the plasma. The only ion damping was through the central third harmonic of the majority deuterium or helium-4 but the single pass damping through this channel was negligible with respect to the electron one. At Ip = 0.75 MA and a central density $n_{e0} \simeq 5 \times 10^{19}$ m^{-3}, a maximum power of 5 MW was coupled. Efficient electron heating was observed, the central temperature rising up to 5.5 keV. High-β_p discharges have also been obtained at Ip = 0.35 MA, $n_{e0} \simeq 4 \times 10^{19}$ m^{-3} when 4 MW were applied, leading to $T_{e0} \simeq$ 4.5 keV and $\beta_p \simeq 1.1$. In these discharges, both the current density (ohmic + bootstrap) and electron temperature profiles (fig. 7) were peaked and up to 45% of the current were carried by the bootstrap current (fig. 6). An increase of the magnetic shear in the gradient region led to improved global confinement as in the LHEP regime and H_{RLW} factors up to 2 were obtained (fig.5). As shown in figure 8, H_{RLW} scales linearly with power and increases at low plasma current. In fact, in both LH and FW high-β_p discharges, the confinement enhancement and the bootstrap current fraction scale roughly linearly with β_p and $\beta_p(a/R)^{1/2}$, respectively. Interestingly, the bootstrap scaling is larger than previously obtained on other Tokamaks in which a significant fraction of the plasma energy was carried by fast ions (fig. 6).

Antenna phasing experiments have started [12] in the aim of studying fast wave current drive (FWCD). Up to 4 MW were coupled to 0.75 MA discharges with a 90° phasing, with little degradation of the electron heating ($T_{e0} \simeq 4$ keV). At lower plasma current (0.4 MA) current drive effects could be more easily assessed from time dependent simulations of the discharge (CRONOS). In order to reproduce the evolution of the experimental signals (loop voltage, magnetic measurements, Faraday rotation angles, ...), for 90° co-current phasing, a total non-inductive current of about 170 kA must be assumed consisting of 90 kA bootstrap and therefore 80 kA driven by the fast wave. Figure 9 shows the result of a phase scan. The agreement with our full wave code simulations (ALCYON [13]) is fairly good, although the experimental current deposition profile which best reproduces the discharge evolution is slighly broader than predicted.

4. RADIATIVE LAYERS IN THE PRESENCE OF AN ERGODIC EDGE

The ergodic divertor (ED) installed on TORE SUPRA has already shown interesting properties regarding MHD stabilization and impurity control. Here we shall describe a third aspect of the ED physics, namely its capability of producing stable radiative layers. For steady-state or long-pulse operation, the heat flux on plasma facing components is strongly reduced when the outer layers of the plasma radiate a large part of the total power. Extensive experiments on such radiative layers produced in the ED configuration were carried out [5] with up to 5.5 MW of ICRH or 3 MW of LH heating.

Various elements were injected into the plasma, producing high edge radiation (D_2, He, CD_4, N_2, Ne, Ar). The small wall retention of neon (especially with the ED on) was found to be important for controlling its concentration from shot to shot and also for reducing the amount of injected gas necessary to reach a given radiated power fraction. As a comparison, for the same radiated fraction, only 1.4×10^{19} neon atoms (among which less than 5×10^{18} are found in the plasma bulk) had to be injected in a plasma containing $\approx 10^{21}$ deuterium atoms whereas nitrogen required the injection of 8×10^{20} atoms. Thus, dense and cold stable layers located mainly on the low field side (i.e. close to the divertor) radiated at least 80 % (25% of which from neon) of the total 7 MW (ohmic + ICRH) power. An example of such a discharge is shown on figure 10. The neon concentration in the plasma core remained below 1% ($\Delta Z_{eff} = 1$). Pushing the radiated fraction higher led to an extension of the radiating layer towards the high field side and to plasma detachment on the low field side. ICRH coupling was then reduced thus leading to a more unstable situation.

Comparing the high radiated fractions obtained in the ED and outboard limiter configurations, large differences were noted [5]. The limiter configuration requires about ten times more neon injection than the ED one for a similar radiative loss increase of about 1 MW (fig. 11). This led however still to central concentrations of about 1%, due to a larger apparent screening of the injected species in the limiter case. Indeed, neon wall retention was higher in the limiter case, probably because the higher energy of impinging ions led to deeper wall penetration. Consistently, the after-shot decay time of the neon pressure was longer (50 s versus 20 s in the ED case). Finally, in the limiter case, radiation fractions higher than 70% led to the production of MARFE's on the high field side and eventually to disruptions.

Infrared thermography of the ergodic divertor neutralizer plates shows the large reduction of the convected heat flux in the presence of a radiating layer (fig. 12). Active pumping has shown a similar efficiency in both limiter and

ED configurations. At the highest radiation levels, when reaching plasma detachment, the pressure drops significantly in the pumping chamber, thus reducing the pumping capability.

5. HEAT AND PARTICLE EXHAUST

Heat and particle exhaust studies with other actively cooled plasma facing components have been pursued [14]. The steady-state heat removal capability of the 12 m^2 graphite inner wall allowed to inject 3.2 MW during 62 seconds (200 MJ). A very good accuracy in the tile alignment (0.5 mm) is necessary to avoid overheating of protruding edges.

A set of modular pump limiters (1 equatorial and 6 bottom ones) provides an alternate means for achieving both heat and particle removal. As for all other components including the ED, the pumping efficiency of these limiters increases roughly as the square of the plasma density. Maximum power loads of 0.8 MW could be deposited during 9 s on the 0.3 m^2 outboard limiter (3 MW/m^2 mean, 17 MW/m^2 peak) and 0.6 MW during 6 s on a 0.12 m^2 vertical one (4 MW/m^2 mean, 8 MW/m^2 peak). Three vertical limiters used simultaneously allowed to extract 1.2 MW during 25 seconds. Thermal equilibrium was reached after 5 and 2 seconds for the horizontal and vertical limiters respectively (fig. 13).

6. CONCLUSION AND FUTURE PROSPECTS

Promising results have been obtained regarding both the obtention of improved confinement regimes and of highly radiating layers. First experiments on Fast Wave electron heating and current drive have been very encouraging. They confirmed the beneficial effect of increasing the magnetic shear in the gradient region of the discharge for reducing the anomalous heat transport, as was obtained also with LHCD. Progress towards steady-state high-β_p operation is a challenge for the future and an open question relates to the shape of the current density profile in the plasma core. In principle, both hollow (LHEP) and peaked (FWCD) profiles can be produced in steady-state together with a large fraction of bootstrap current. One of the aims of future high-β_p experiments will be to compare the transport and stability properties of peaked and shear-reversed configurations, and their respective merits for "advanced Tokamak" operation.

As far as heat and particle exhaust is concerned, stable radiative layers (≥80% radiation) have been successfully obtained through neon injection in the ergodic divertor configuration. The production of a magnetically ergodized plasma edge turns out to have a set of interesting properties for high power

steady-state Tokamak operation (radiative layers, pumping, impurity control, MHD stabilization). The ergodic divertor thus appears as an attractive alternative to the conventional poloidal divertor and will deserve further studies.

The programme will continue along the following lines :

i) Improvement of the machine capability to operate with radiative layers, and of the associated diagnostic equipment. In particular a reinforced ergodic divertor is being designed which should be compatible with a convected power level of about 10 MW.

ii) Improvement of plasma facing components to increase the heat and particle exhaust capability, in both radiation and conduction regimes. A new generation of high flux actively cooled components is now under study.

iii) Steady-state scenarios using current drive and current profile control techniques, and also high β_p regimes.

Progress along these three lines should allow to operate the machine with discharge durations well beyond 100 seconds ("TORE SUPRA CONTINU" project).

Acknowledgements

Fruitful collaborations with many institutions listed in the appendix are warmly acknowledged.

REFERENCES

[1] GARBET, X., et al., IAEA-CN-60/A-2-III-4, these Proceedings.

[2] DUBOIS, M., in Proceedings of the 21st European Conference on Controlled Fusion and Plasma Physics, Montpellier (1994).

[3] REBUT, P.H., LALLIA, P., WATKINS, M., in *Plasma Physics and Controlled Nuclear Fusion Reasearch*, Proceedings of the 12th International Conference, Nice, 1988 (IAEA, Vienna,1989), Vol. 2, p. 191.

[4] EQUIPE TORE SUPRA (presented by B. Saoutic), in Proceedings of the 21st European Conference on Controlled Fusion and Plasma Physics, Montpellier (1994).

[5] EQUIPE TORE SUPRA (presented by A. Grosman), IAEA-CN-60/A-4-II-6, these Proceedings.

[6] GERAUD, A., et al., in Proceedings of the 21st European Conference on Controlled Fusion and Plasma Physics, Montpellier (1994).

[7] HOANG, G.T., et al., in Proceedings of the 21st European Conference on Controlled Fusion and Plasma Physics, Montpellier (1994).

[8] HUYSMANS, G., PARAIL, V., private communication.

[9] CHALLIS, C., et al., Nucl. Fus. 33 (1993) 1097.

[10] ISHIDA, S., et al., Phys. Rev. Lett. 68 (1992) 1531.

[11] ZARNSTORFF, M.C., et al., Phys. Rev. Lett. 60 (1988) 1306.

[12] EQUIPE TORE SUPRA (presented by B. Saoutic), IAEA-CN-60/A-3-I-6, these Proceedings.

[13] BECOULET, A., et al., to be published in Phys. Plasmas.

[14] EQUIPE TORE SUPRA (presented by D. Guilhem), IAEA-CN-60/A2/4-P-17, these Proceedings.

APPENDIX

TORE SUPRA Team and collaborations :

G. Agarici, J. P. Allibert, J.M. Ané, R. Arslanbekov, S. Balme, B. Bareyt, V. Basiuk, P. Bayetti, L. Baylor [1], B. Beaumont, R. Becherer, A. Bécoulet, M. Benkadda [2], G. Berger-By, S. Bério, D. Bessette, P. Bibet, J.P. Bizarro [3], G. Bon-Mardion, P. Bonnel, J. Boscary, J.M. Bottereau, F. Bottiglioni, S. Brémond, R. Brugnetti, R. V. Budny [4], Y. Buravand, H. Capes, J.J. Capitain, J.L. Carbonnier, J. Carrasco, C. Chamouard, P. Chappuis, D. Chatain, E. Chatelier, M. Chatelier, J.H. Chatenet [5], D. Ciazynski, F. Clairet, L. Colas, J.J. Cordier, A. Côté [6], J.P. Coulon, B. Couturier, J.P. Crenn, P. Cristofani, C. Deck, P. Decool, B. De Gentile, H. Demarthe, J. C. De Haas, C. De Michelis, P. Deschamps, C. Desgranges, P. Devynck, L. Doceul, C. Doloc, M. Dougnac, H.W. Drawin, M. Druetta [7], M. Dubois, J.L. Duchâteau, T. Dudok de Wit, L. Dupas, D. Edery, D. Elbèze, D. Escande, J.L. Farjon, I. Fidone, J.R. Ferron [8], M. Fois, C. Forrest [8], C.A. Foster [1], D. Fraboulet, D. Frigione [9], V. Fuchs [6], M. Fumelli, B. Gagey, L. Garampon, X. Garbet, E. Gauthier, A. Géraud, F. Gervais [10], P. Ghendrih, C. Gil, G. Giruzzi, M. Goniche, R. Gravier, B. Gravil, M. Grégoire, D. Grésillon [10], C. Grisolia, A. Grosman, D. Guilhem, B. Guillerminet, R. Guirlet, L. Guiziou, J. Harris [1], G. Haste [1], P. Hennequin [10], F. Hennion, P. Hertout, W.R. Hess, M. Hesse, G.T. Hoang, J. Hogan [1], T. Hutter, J. Idmtal, R. Isler [1], C. Jacquot, B. Jager, F. Jequier, E. Joffrin, J. Johner, J.Y. Journeaux, P. Joyer, S. M. Kaye [4], C. Klepper [1], F. Kazarian, K. Kupfer [8], H. Kuus, D. Lafon, P. Laporte, J. Lasalle, L. Laurent, C. Laviron, G. Leclert [11], P. Lecoustey, A. Ledyankine, C. Leloup, Y.Y. Li [12], P. Libeyre, M. Lipa, X. Litaudon, T. Loarer, P. Lotte, J.F. Luciani [5], T. Lutz [13], R. McGrath [13], P. Magaud, A. Mahdavi [8], R. Magne, G. Martin, A. Martinez, E.K. Maschke, R. Masset, M. Mattioli, G. Mayaux, Y. Michelot, P. Mioduszewski [1], J. Misguich, P. Mollard, P. Monier-Garbet, D. Moreau, F. Moreau, J.P. Morera, B. Moulin, D. Moulin, M. Moustier, R. Nakach, F. Nguyen, R. Nygren [13], P. Ouvrier-Buffet, L. Owen [1], M. Pain, J. Pamela, F. Parlange, G. Pastor, R. Patris, M. Paume, J. Payan, A.L. Pecquet, B. Pégourié, Y. Peysson, D. Piat, J.M. Picchiottino, P. Platz, C. Portafaix, M. Prou, L. Qualls [1], A. Quemeneur [10], J.M. Rax [14], H. Renner [15], G. Rey, P. Riband, B. Rothan, P. Roussel, S.A. Sabbagh [16], R. Sabot, F. Samaille, A. Samain, B. Saoutic, J. Schlosser, A. Seigneur, J.L. Segui, F. Smits, K. Soler, P.G. Sonato [17], Y. Stephan [18], M. Talvard, J. M. Theis, C. E. Thomas [1], S. Tobin [13], G. Tonon, A. Torossian, A. Truc [10], E. Tsitrone, B. Turck, S. Turlur, T. Uckan [1], G. Urquijo, J.C. Vallet, J. Valter, D. VanHoutte, A. Verga [2], D. Vézard, H. Viallet, J. Weisse, R. White [4], T. Wijnands, M. Zabiego, X.L. Zou.

---

1) Oak Ridge National Laboratory, Oak Ridge, Tennessee, USA.
2) Equipe Turbulence Plasma, Institut Méditerranéen de Technologie, Marseille, France.
3) Instituto Supérior Tecnico, Association EUR-IST, Lisboa, Portugal.
4) Princeton Plasma Physics Laboratory, Princeton University, New Jersey, USA.
5) Centre de Physique Théorique, Ecole Polytechnique, France.
6) Centre Canadien de Fusion Magnétique, Varennes, Québec, Canada.
7) Laboratoire de Traitement du Signal et d'Instrumentation, CNRS, St Etienne, France.
8) General Atomics, San Diego, California, USA.
9) C.R.E. Association EUR-ENEA, Frascati, Italy.
10) Physique des Milieux Ionisés, Ecole Polytechnique, Palaiseau, France.
11) L.P.M.I., Université de Nancy I, Vandœuvre les Nancy, France.
12) Institute of Plasma Physics, Hefei, China.
13) Sandia National Laboratories, Albuquerque, New Mexico, USA.
14) Université Paris XI, Orsay, France.
15) Max Planck Institut fur Plasmaphysick, Association EUR-IPP, Garching, Deutschland.
16) Department of Applied Physics, Columbia University, New York, New York, USA.
17) C.S.Gas Ionizzati, Association EUR-ENE-CNR, Padova, Italy.
18) CISI Ingénierie, Centre d'Etudes de Cadarache, France.

FIGURE CAPTIONS

Fig.1. Behaviour of the magnetic fluctuations in ohmic and auxiliary heated discharges as a function of the central density. The parameters of these helium plasmas are I_p = 1.3 MA, B_t = 3.7 T, q_a = 3.

Fig.2. (a) Temperature profiles with (open) and without (black) the ergodic divertor. Triangles correspond to measurements by Thomson scattering and squares are from Langmuir probe measurements. The (helium) plasma parameters are $\langle n_e \rangle = 3.5 \times 10^{19}$ m^{-3}, I_p = 1.4 MA, B_t = 3.2 T, q_a = 3.

(b) Radial profile of the reduction of the turbulence level with ergodic divertor operation, measured by reflectometry.

(c) Evolution of the squared density fluctuation level measured by coherent scattering for a wave vector k = 400 m^{-1}.

Fig. 3. Time evolution of the plasma parameters for a typical shot with injection of a fast pellet (2 km/s, 2.5×10^{21} deuterium atoms) and ICRH.

Fig.4. Stationary LHEP discharge : I_p = 0.8 MA, B_t = 4 T, $n_e(0) = 2.7 \times 10^{19}$ m^{-3}, P_{LH} = 3 MW.

(a) Current density profile at time t = 8s. Total and LH-driven currents are obtained with magnetic reconstruction (IDENT-D) and ray-tracing (Bonoli-Fuchs) codes.

(b) Time evolution of the electron thermal diffusivity (χ_e), central safety factor (q_0) and central electron temperature (T_{e0}).

Fig.5. Confinement improvement factor, H_{RLW}, versus β_p : L-mode (+), LHEP (x), FWEH (o), combined LHEP/FWEH (*).

Fig. 6. Bootstrap current fraction as a function of $\beta_p(a/R)^{1/2}$, in TORE SUPRA ohmic plasmas (+), during LHEP (x), and with FWEH (o). Also shown are data from JET, JT-60 and TFTR [9-11].

Fig. 7. Electron temperature profile during ohmic and FWEH and Fast Wave power deposition profile predicted by ALCYON (shaded).

Fig. 8. Confinement improvement factor versus fast wave power.

Fig. 9. Fast wave driven current versus antenna phasing. Squares correspond to experimental results and triangles to ALCYON predictions.

Fig. 10. Time evolution of the main plasma parameters during a radiative layer experiment with ICRH.

Fig. 11. Radiated power fraction versus the number of injected neon atoms in the limiter and ergodic divertor configurations.

Fig. 12. Infrared thermographic image of an ergodic divertor neutralizer, (a) without a radiative layer, (b) with a radiative layer. (c) Time evolution of the thermal flux on the ergodic divertor neutraliser plates and ICRH power.

Fig. 13. (a) Time evolution of three representative locations on the front face of the outboard limiter when the extracted power is 800 kW.

(b) Time evolution of three representative locations on a vertical limiter when the extracted power is 400 kW.

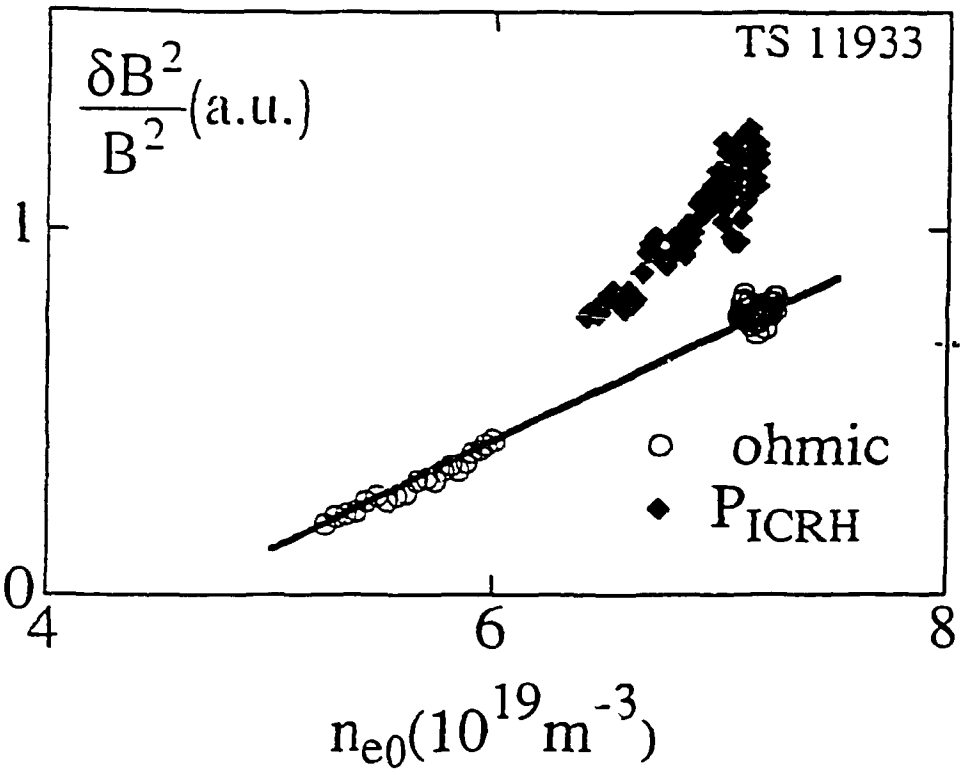

Figure 1

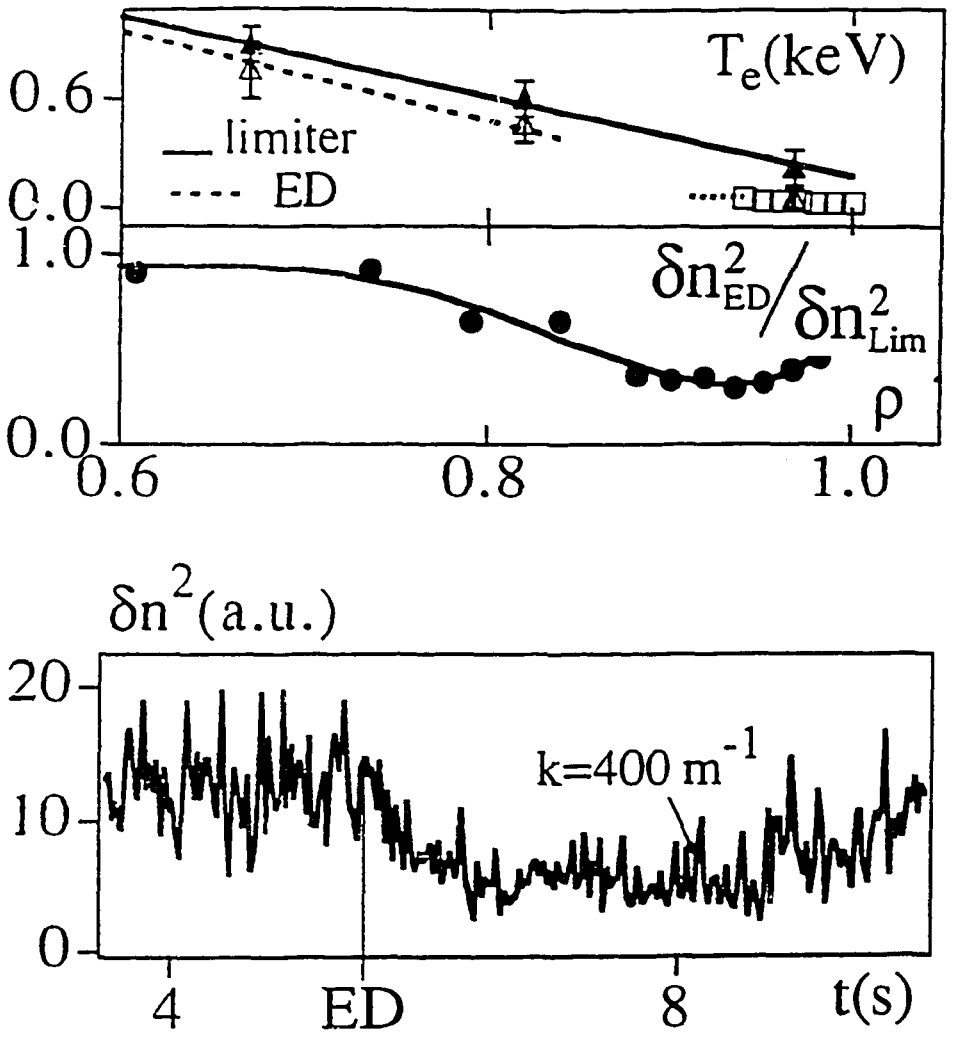
T_e(keV)
0.6
0.0
limiter
ED
1.0
$\delta n^2_{ED}/\delta n^2_{Lim}$
0.0
ρ
0.6
0.8
1.0
δn^2(a.u.)
20
10
0
k=400 m^{-1}
4
ED
8
t(s)

Figure 2

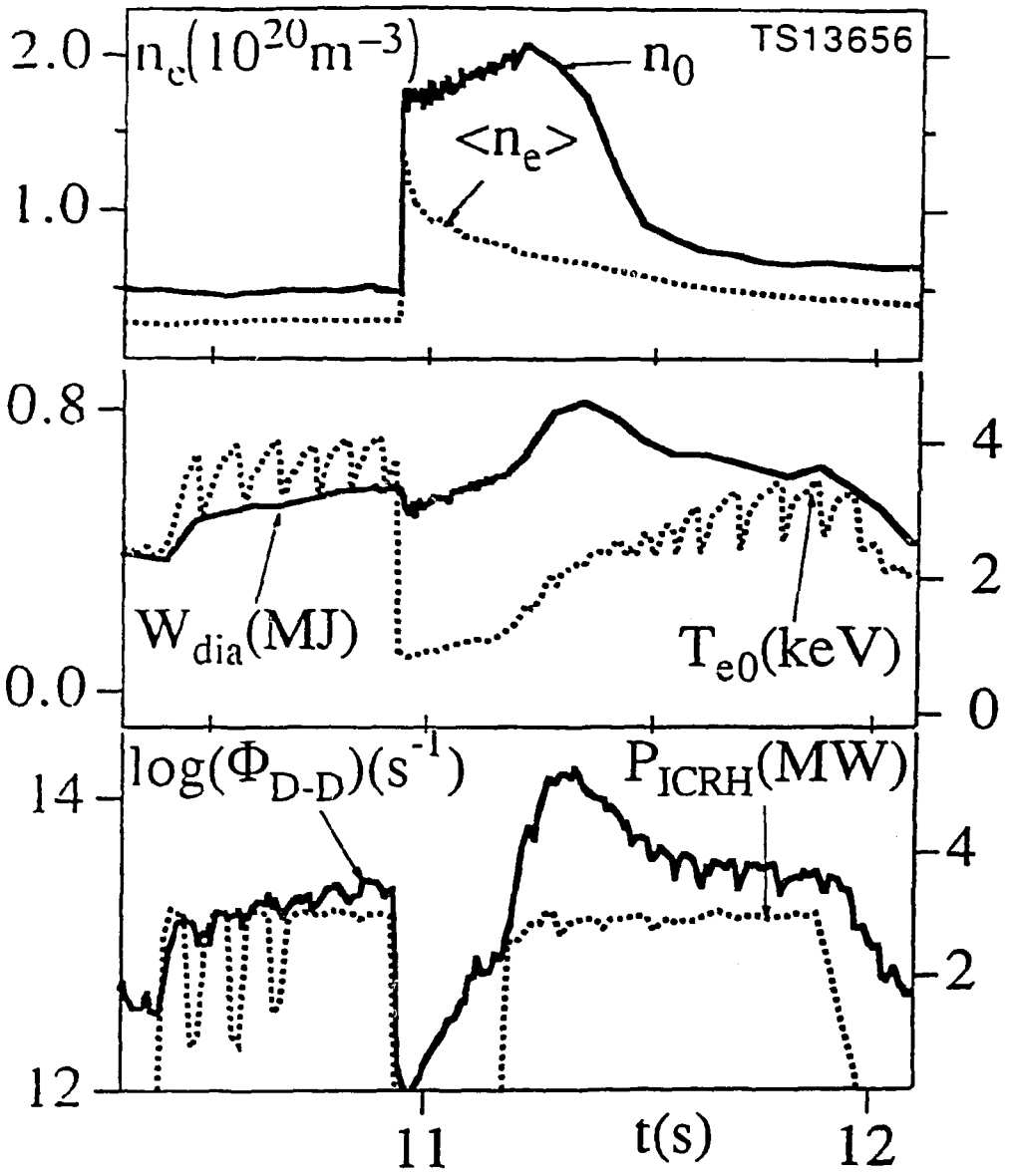
2.0
1.0
$n_e(10^{20}m^{-3})$
n_0
TS13656
$<n_e>$
0.8
0.0
$W_{dia}(MJ)$
$T_{e0}(keV)$
4
2
0
14
12
$\log(\Phi_{D-D})(s^{-1})$
$P_{ICRH}(MW)$
4
2
11
t(s)
12

Figure 3

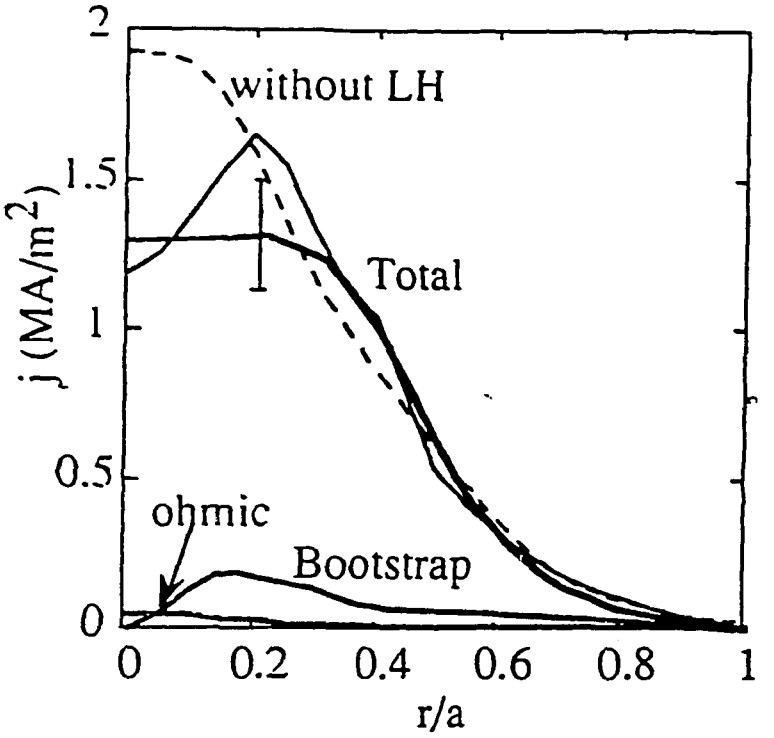
without LH
Total
ohmic
Bootstrap
j (MA/m2)
r/a

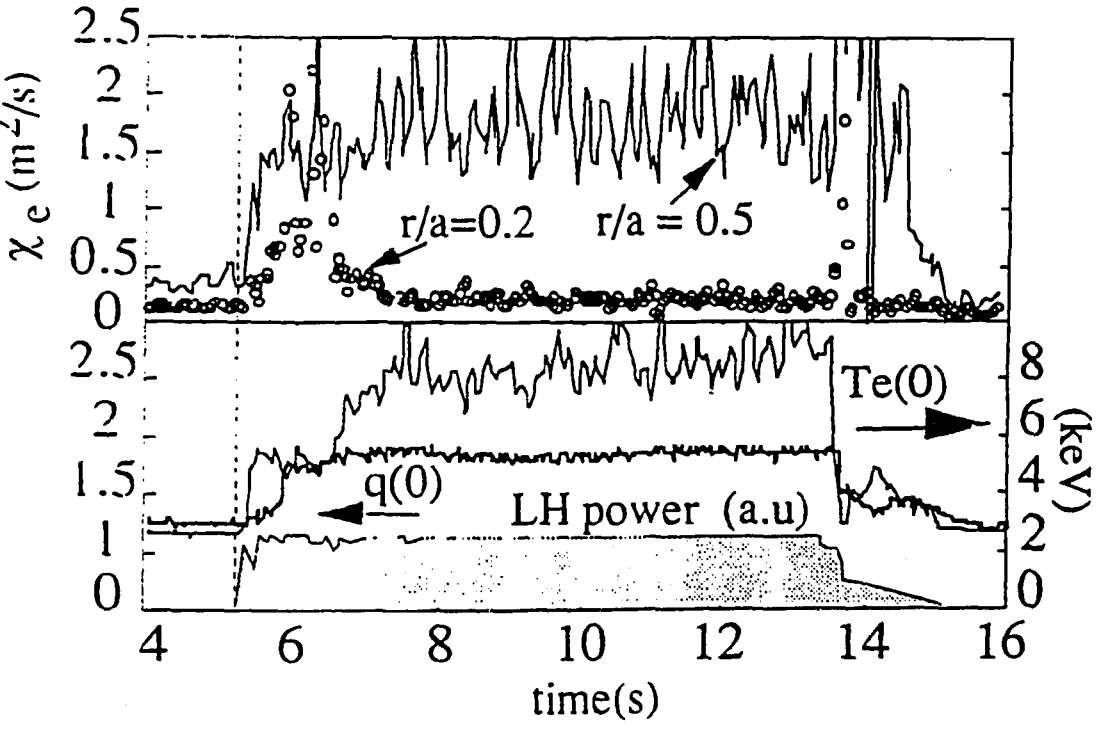
χe (m2/s)
r/a=0.2
r/a = 0.5
Te(0)
q(0)
LH power (a.u)
(keV)
time(s)

Figure 4

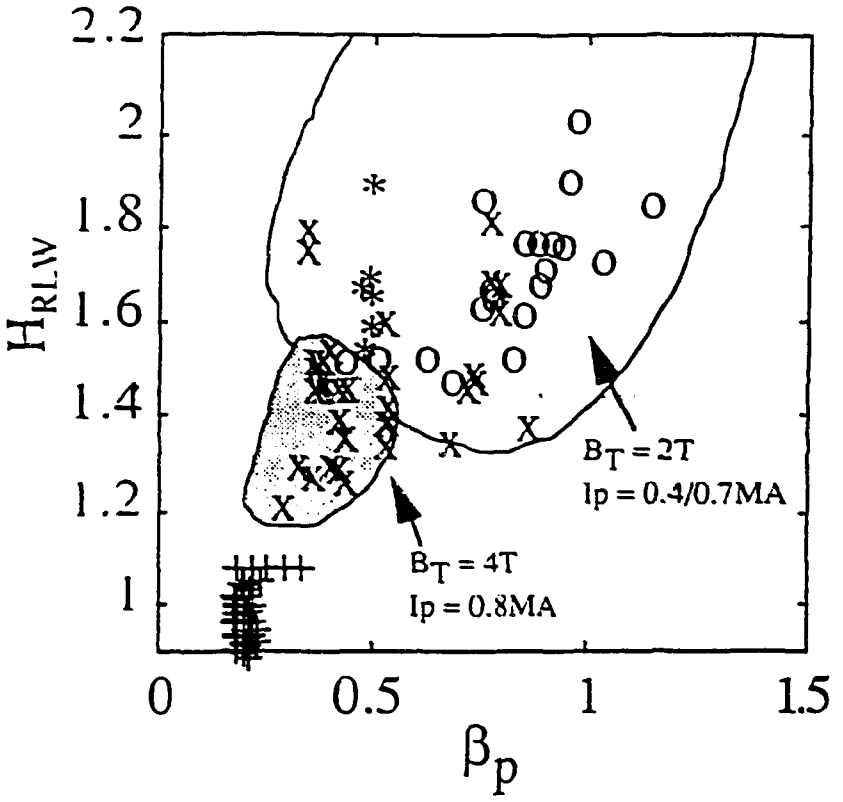

Figure 5

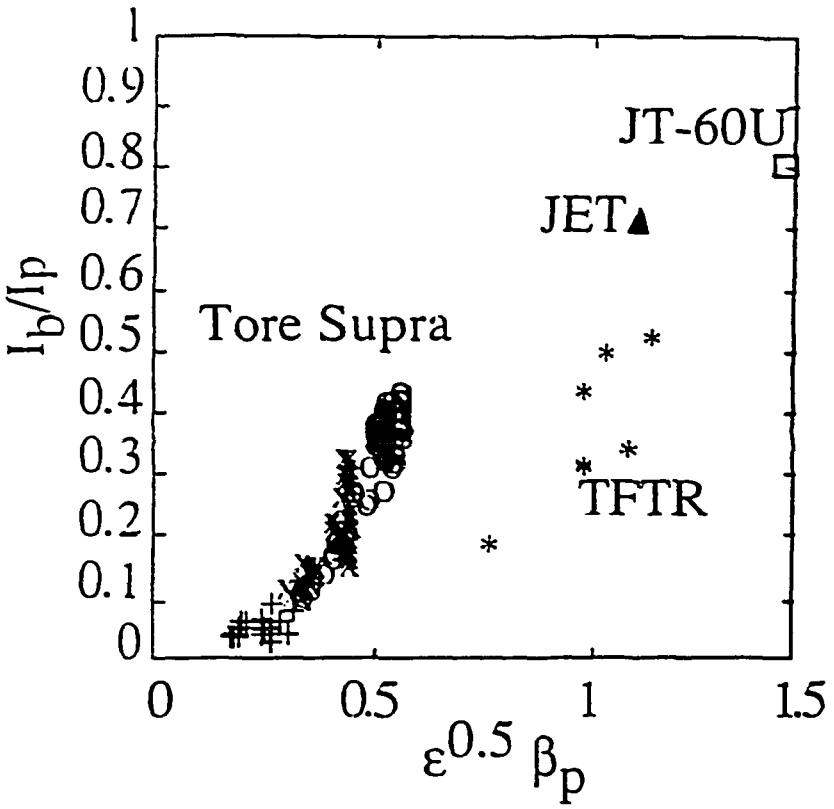
JT-60U
JET
Tore Supra
TFTR
I_b/I_p
$\varepsilon^{0.5}\,\beta_p$
0
0.1
0.2
0.3
0.4
0.5
0.6
0.7
0.8
0.9
1
0.5
1
1.5

Figure 6

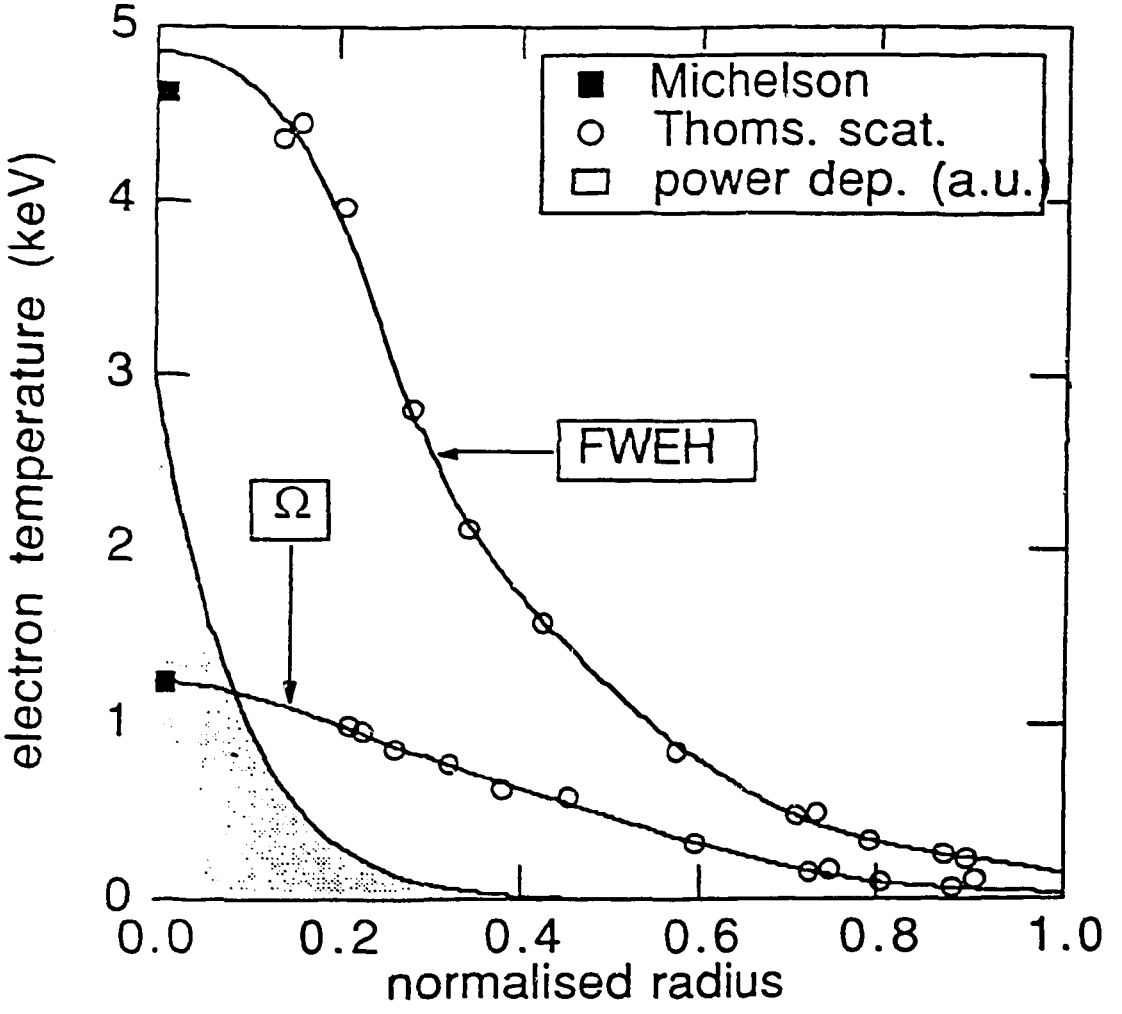
Michelson
Thoms. scat.
power dep. (a.u.)
FWEH
Ω
electron temperature (keV)
normalised radius
0
1
2
3
4
5
0.0
0.2
0.4
0.6
0.8
1.0

Figure 7

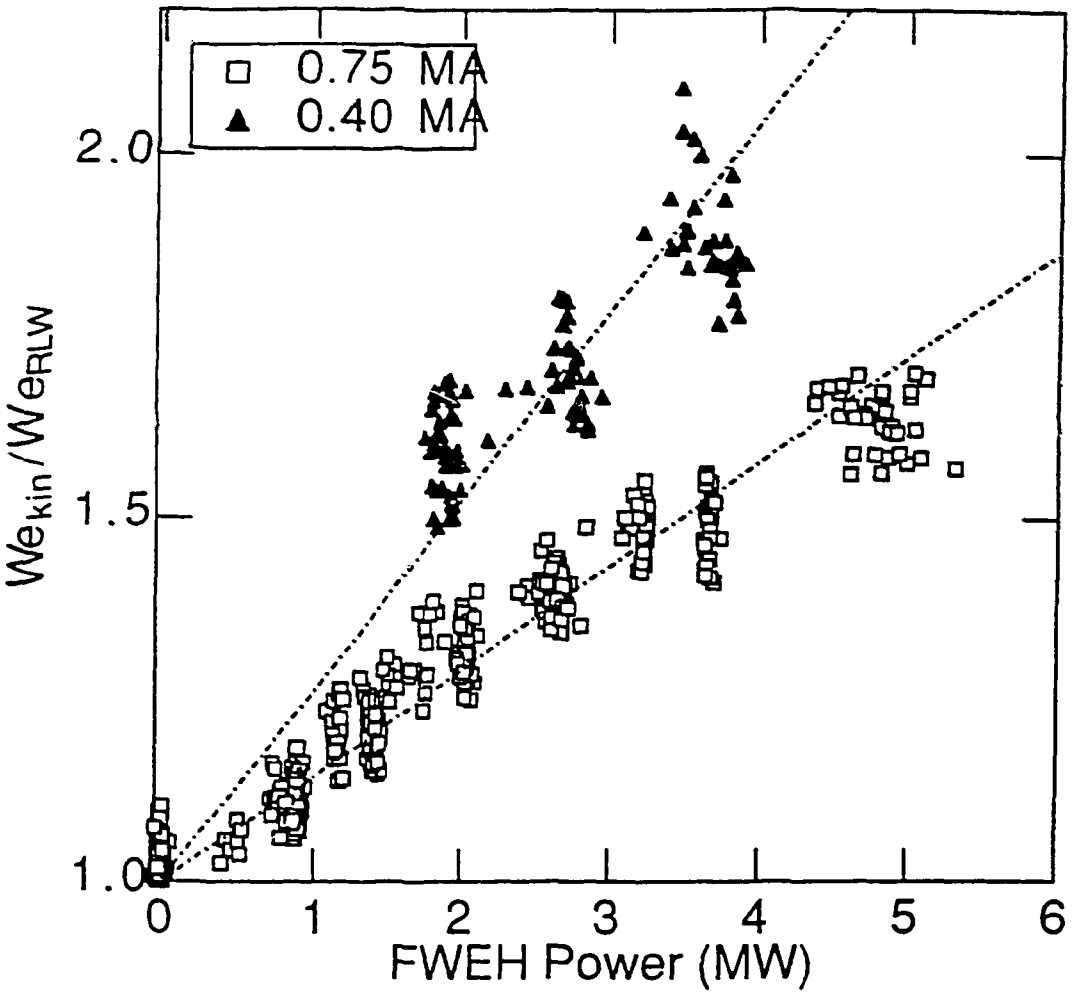

Figure 8

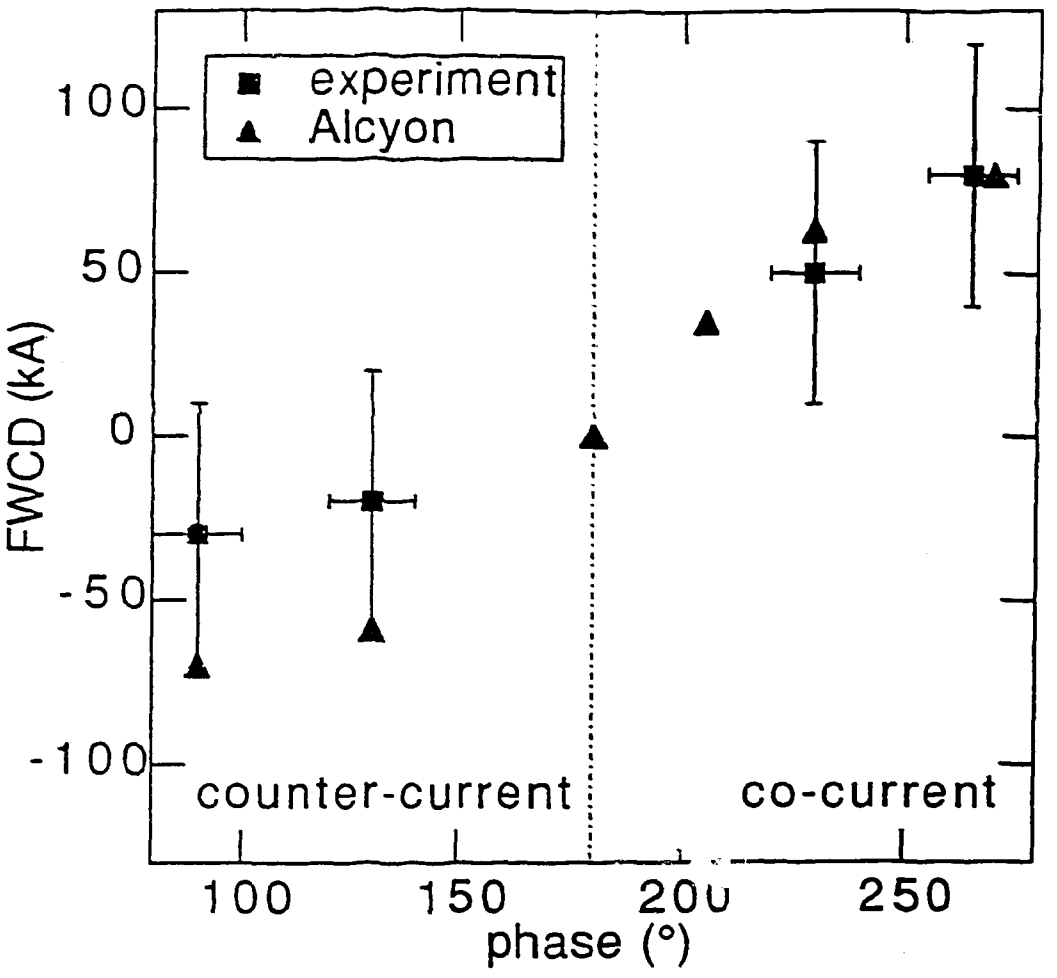
experiment
Alcyon
100
50
0
-50
-100
FWCD (kA)
counter-current
co-current
100
150
200
250
phase (°)

Figure 9

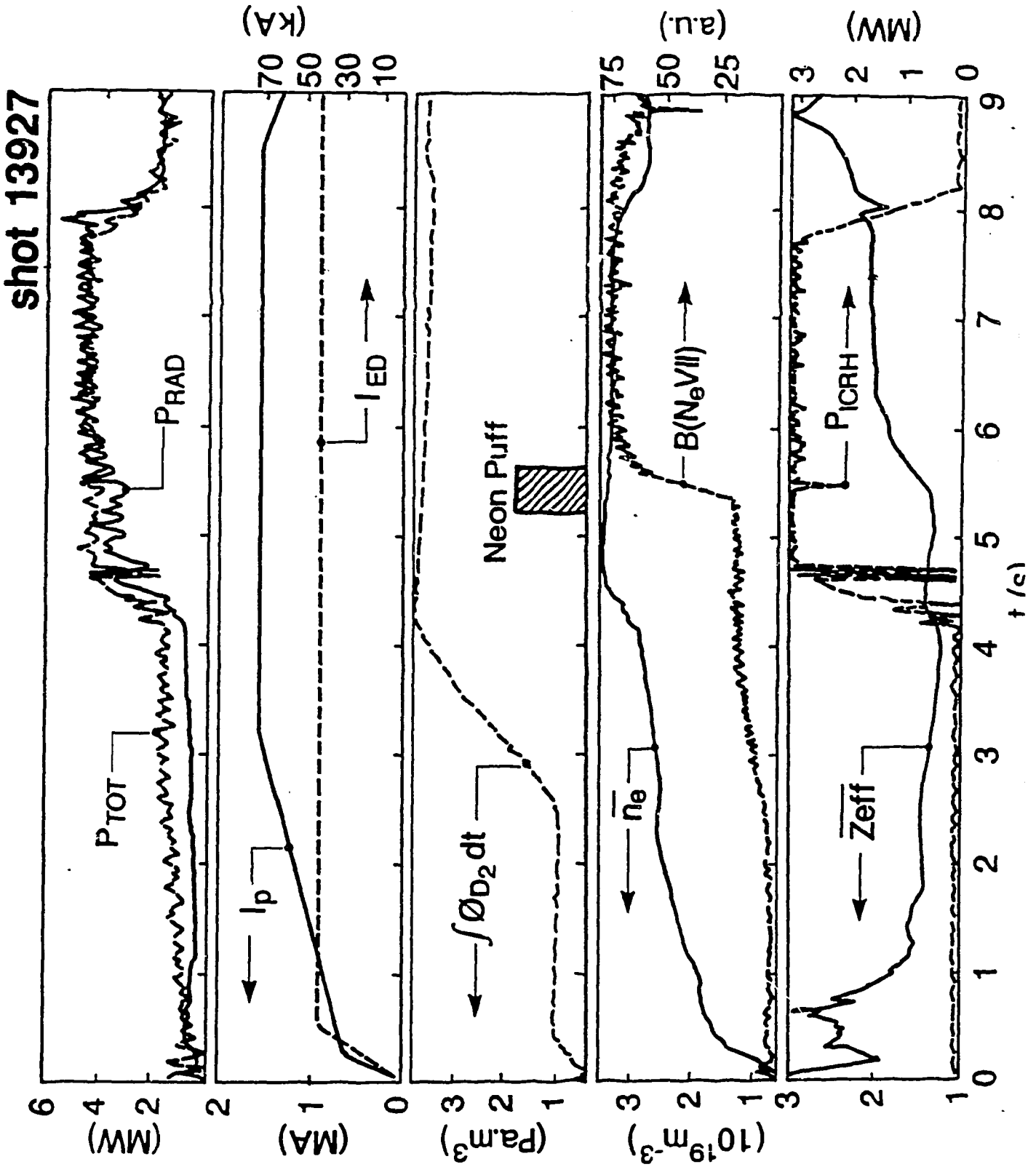
shot 13927
P_TOT
P_RAD
I_p
I_ED
Neon Puff
∫Ø_D2 dt
n̄_e
B(N_eVII)
Z̄eff
P_ICRH
(MW)
(MA)
(kA)
(Pa.m³)
(10¹⁹m⁻³)
(a.u.)
(MW)
t (s)

FIGURE 10

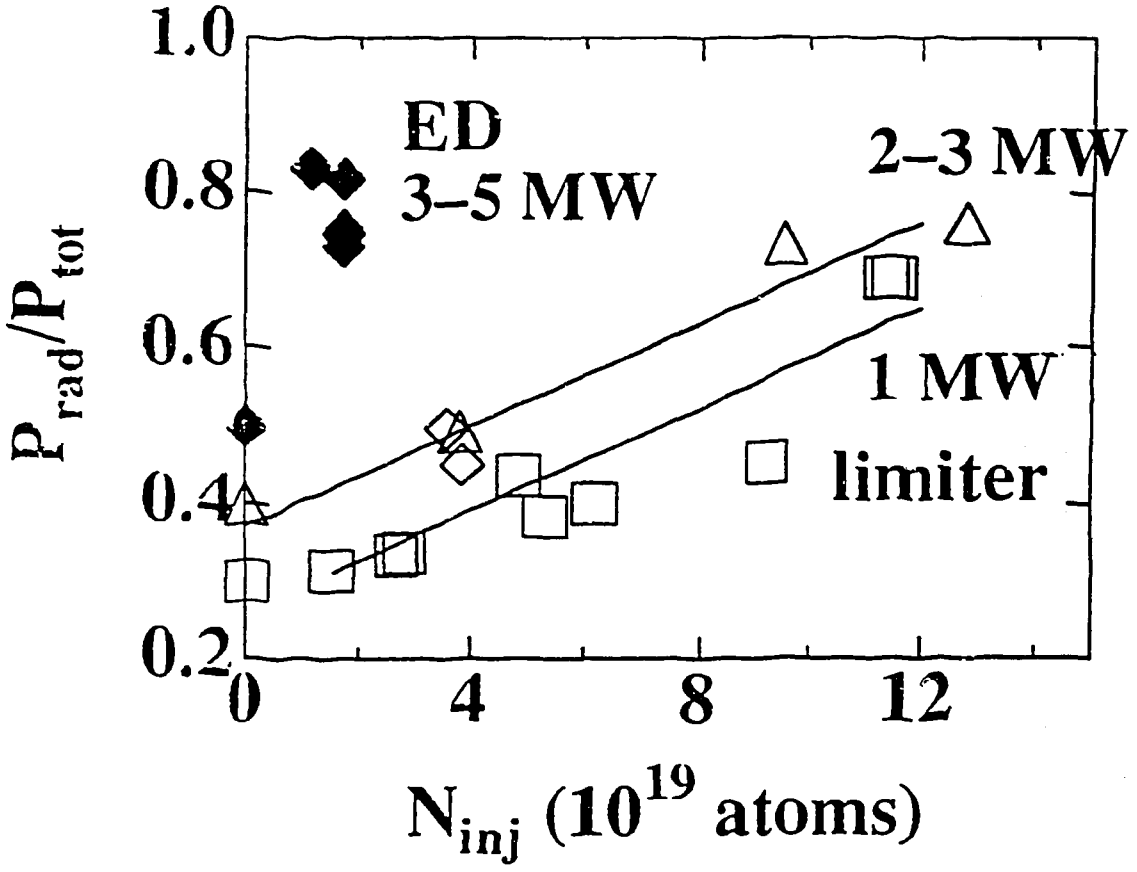
1.0
0.8
0.6
0.4
0.2
0
4
8
12
ED
3–5 MW
2–3 MW
1 MW
limiter
P_{rad}/P_{tot}
N_{inj} (10^{19} atoms)

Figure 11

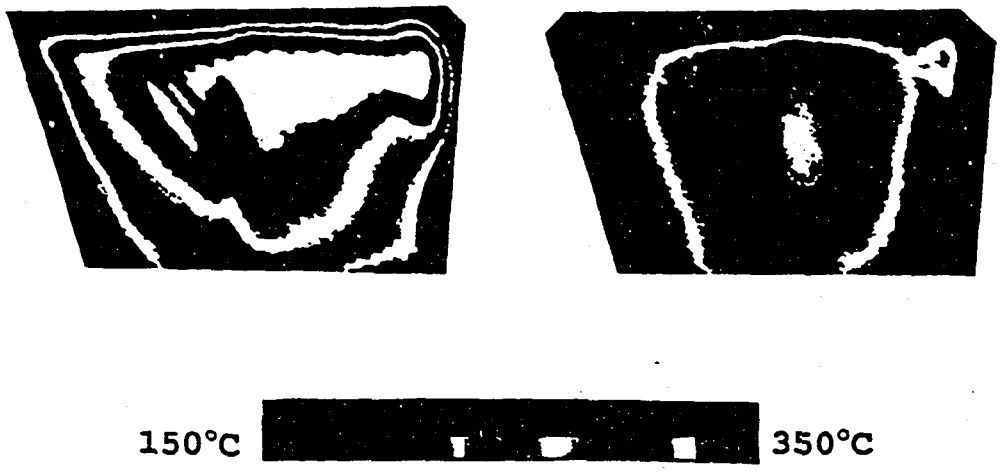
150°C
350°C
Thermal flux on ED neutralizer
SHOT 13927
Flux (MW/m2)
P ICRH (MW)
Neon inj.
0
1
2
3
4
5
6
7
8
0
2
4
6
8
10
t (s)

FIGURE 12

a)

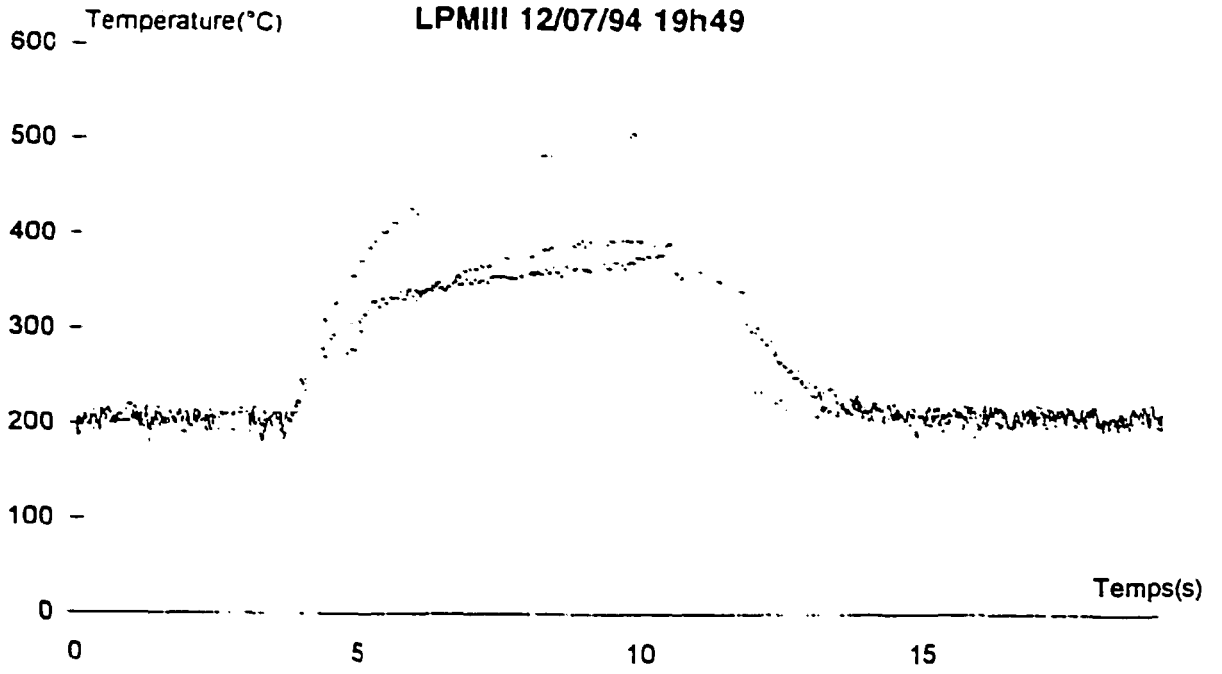
Temperature(°C)
LPMIII 12/07/94 19h49
600
500
400
300
200
100
0
Temps(s)
0
5
10
15

b)

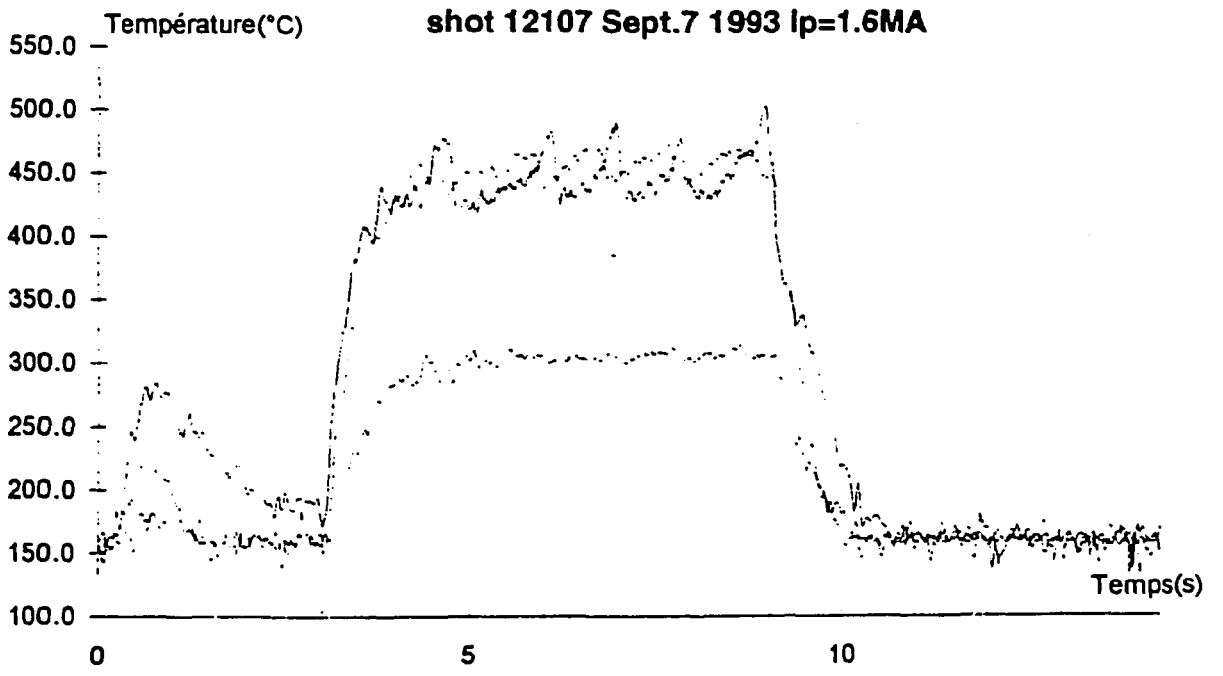
Température(°C)
shot 12107 Sept.7 1993 Ip=1.6MA
550.0
500.0
450.0
400.0
350.0
300.0
250.0
200.0
150.0
100.0
Temps(s)
0
5
10

FIGURE 13